Computational approach for optimal sensor setup

Xiaoping Qian
Kevin G. Harding, MEMBER SPIE
General Electric Company
Global Research Center
Inspection and Manufacturing
 Technologies
Schenectady, New York 12301
E-mail: qian@crd.ge.com

Abstract. Optical metrology has been widely used in quality inspection. However, the sensor setup during part inspection is often done in an *ad hoc* way. This leads to unnecessarily high signal dynamic range. Consequently, optical sensors do not have sufficient light dynamic range capabilities especially for shiny surface measurement. We present a computational approach for optimal sensor setup that takes into account the sensor/part interaction to decrease signal dynamic range and to increase model coverage for structured light or similar optical inspection systems. First, we transform the signal dynamic range issue into a distance problem in a spherical map. We then present novel algorithms on the spherical map to search a near-optimal sensor orientation. Based on this near-optimal orientation, we use a gradient method to obtain the free-optimal solution that gives the lowest possible dynamic range. Experimental results demonstrated that under the optimal orientation, there is lower signal dynamic range and better model coverage. Future work on extending this method to multiple sensor planning, sensor design, and stage design for large part inspection is also discussed. © *2003 Society of Photo-Optical Instrumentation Engineers.* [DOI: 10.1117/1.1566777]

1 Introduction

Over the past two decades, optical measurement has gained increasing popularity in all aspects of manufacturing and quality inspection processes. Despite its wide usage, optical measurement is very sensitive to the relative position and orientation between the part and the sensor. Sensors are often designed/selected without a detailed analysis of geometric and optical properties of the part. This may lead to high signal dynamic range, and consequently poor model coverage and low measurement accuracy. This is especially true for surface inspection with an area sensor, where surfaces may possess different surface finish at different spots. At the smooth and shiny spots, there is high specular reflection and low diffuse reflection. At the rough spots, there is low specular and high diffuse reflection. An area sensor effectively collects all the diffuse reflection within the field of view. Therefore, parts with different surface finish often lead to high signal dynamic range when inspected with area sensors. Two examples are given in Fig. 1, where two grayscale images with underbrightness and oversaturation are shown. Consequently, there are large defective gaps in the corresponding reconstructed 3-D images.

In this paper, we present a computational approach for the optimal sensor setup that takes into account the sensor/part interaction to decrease signal dynamic range and to increase model coverage for structured light or similar optical inspection systems.

A schematic diagram of the measurement system we use is shown in Fig. 2. In this measurement system, two cameras are deployed next to a laser source in a triangulation-type system. The part to be inspected is a blade such as those used in compressors or turbines. By varying the standoff distance (SD), baseline distance (BD), and three orientation angles (azimuth, elevation, and twist), the cameras receive different dynamic ranges of light, resulting in different model coverage.

The contributions of this paper include that we find the best sensor setup for multiple cameras simultaneously, while most previous works only consider one camera. In addition, based on novel spherical algorithms developed in this paper, signal dynamic range is explicitly minimized via an optimal sensor setup.

In the remainder of the paper, Sec. 2 reviews the existing methods for optical sensor setup and the related setup techniques in different applications. In Secs. 3 and 4, we present the problem formulation, outline the overall procedures, and detail each step involved in this computational approach. We first transform the dynamic range minimization issue into a camera view angle optimization problem. We then consider the relative orientation of laser and cameras on the blade's spherical map. A geometric reasoning approach is developed to seek the near-optimal setup. Then, an iterative approach is employed to find the optimal setup. Experimental results are presented in Sec. 5 and conclusions in Sec. 6.

2 Literature Review

The part and sensor setup issue is an important problem for 3-D measurement. An overview of 3-D measurement systems and their applications is presented in Ref. 1. Sensor planning considering where the sensor should be placed has been explored from many perspectives. The lighting issues and how parts reflect light for optical measurements in general are discussed in Ref. 2. A general description of ad-
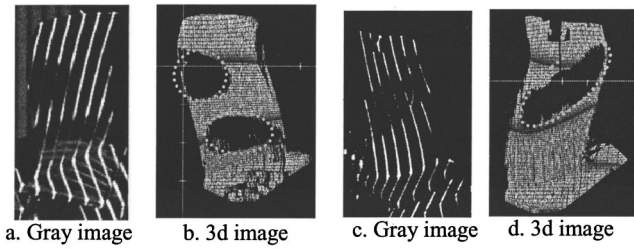
a. Gray image   b. 3d image   c. Gray image   d. 3d image

Fig. 1 Limited sensor dynamic range and poor model coverage.

Fig. 3 Gaussian map of a blade.

vanced laser gage applications including speed and resolution issues is discussed in Ref. 3. Methods for speckle reduction for laser line gages are presented in Ref. 4. A visibility-based approach is presented in Ref. 5. The optimal setup for measurement related to edges is explored in Ref. 6. However, none of these works explicitly explored the setup impact on signal dynamic range even though limited sensor dynamic range remains a challenge for many optical applications. A review of current methods for expanding sensor dynamic range is reported in Ref. 7.

Gaussian mapping is a technique often used to solve setup orientation issues. A Gaussian map is a set of surface normals projected onto a unit sphere. It has been extensively used in many setup applications, such as molding and die processing and ECM machining.[8–10] An algorithm based on central projection of surface normals was developed to obtain the spherical convex hull of the Gaussian map.[8] The complexity of the algorithm is $O(n \log n)$. The algorithm involves rotating point sets to avoid singularities, doing a central projection for the top and bottom halves of the point sets so that they are not close to the equator, and checking to see if they are intersecting. If the point sets do intersect, a great circle needs to be found to separate the two halves. However, due to the complexity in its implementation and the singularity problem when points are close to the equator, an alternate algorithm is developed in this paper.

Gaussian mapping is also used in layered manufacturing to find an optimal build orientation to increase surface quality.[11] It has also been used to determine the fewest number of setups for optical inspection. A near-optimal view planning method for optical sensors is presented in Ref. 12. For a given object, the Gaussian map was used to find the minimal number of orientations so that the object could be fully covered. A method for the Gaussian map calculation for a free-form surface is reported in Ref. 13.
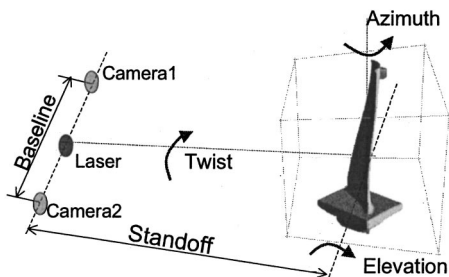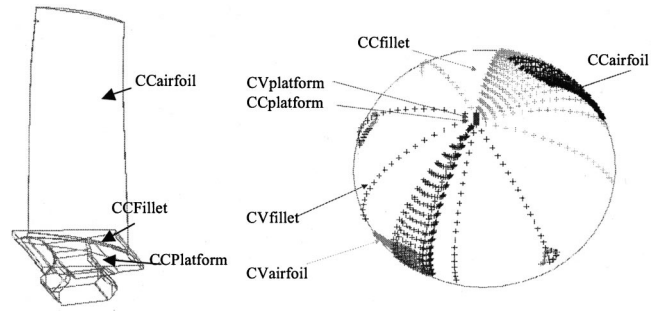
The problem addressed in this paper differs from the above in that it finds the best sensor setup for signal dynamic range minimization as opposed to finding the fewest number of setups. It considers multiple cameras simultaneously while most previous works only consider one camera. It develops novel spherical algorithms for spherical convex hull and minimal maximum distance search. For example, Fig. 3 shows a blade and its corresponding Gaussian map. The concave surface, fillet, and platform on the concave side are to be inspected in one setup, and the convex surface, fillet, and platform on the convex side are to be inspected in a second setup. The methodology presented in this paper finds an optimal setup for each side.

3 Problem Formulation

The system we consider in this paper is shown in Fig. 2. The solution derived for this system can be adapted to other systems accordingly. A typical laser inspection system has five setup parameters: standoff distance SD, baseline distance BD, part azimuth and elevation angles, and camera twist angle. The objective is to adjust these parameters to increase the model coverage by minimizing the signal dynamic range on each camera, without degrading the system's ability to make the desired measurements. That is, simply making all the angles very small is not a viable option since the resolution of the system per triangulation effect would then be very poor. So, there must exist a sufficiently large angle between the cameras to make the measurements, while also keeping the dynamic range of light levels within acceptable limits.

In Fig. 4, we highlight one point p_i, its surface normal N, left camera view vector (LCV), right camera view vector
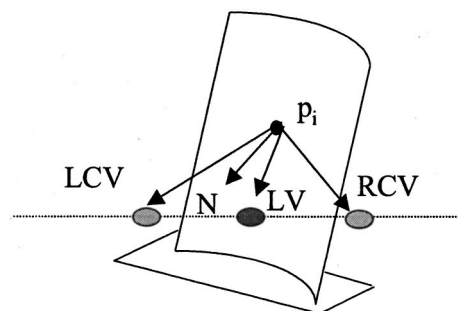

Fig. 2 Schematic diagram of light gauge measurement system.

Fig. 4 Laser incidence angle and camera view angles.

(RCV), and laser vector (LV). The camera view angle is $a \cos(N \cdot LV)$ and the laser incident angle is $a \cos(CV \cdot N)$.

The light intensity received by a camera can be represented by:[14]

$$I = \frac{\cos^2 \theta * k_c}{(D_{SD}^2 + D_{BD}^2) * k_d}.$$ (1)

In this equation, θ is a camera view angle, k_c is the aperture length factor, and k_d is diffusion coefficient.

As shown in Eq. (1), signal dynamic range is predominantly determined by the camera view angle. The standoff distance and baseline distance only have a marginal effect. For a typical optical system, the ratio between the standoff distance and the depth of volume is larger than 5:1. Assuming a baseline that is 5 times the depth of the volume being measured, then Eq. (1) can be simplified to:

$$I = \frac{\cos^2 \theta * k_c}{k_{SD\_BD} * k_d}.$$

In the above equation, the coefficient k_{SD_BD} represents the distance factor, which is approximately a constant factor for all the points within the measurement volume. The deviation of k_{SD_BD} is less than 2% throughout the measurement volume.

Dynamic range is defined as the ratio of maximum light intensity and minimum light intensity received by each camera:

$$DR = \max(I_{i=1,n}) / \min(I_{i=1,n}).$$ (2)

By calculating Eq. (2) for all the surface points ($i = 1...n$) and for different diffuse coefficients ($k_d = 1$ for complete diffuse reflection, $k_d = 0.05$ for diffuse reflection at shiny spots), we can obtain signal dynamic range received by each camera. From Eq. (2), for any given SD and BD, the issue of minimizing dynamic range can be considered as an issue of minimizing camera view angles.

In order to find the optimal setup to minimize the camera view angles for all the cameras, we transfer all five setup parameters into the part's Gaussian map. Figure 3 shows an airfoil surface and a platform surface of a turbine blade that needs to be inspected. The surface normals as mapped onto the Gaussian map are shown on the right side of Fig. 3.

All five setup parameters can be represented in the Gaussian map (see Fig. 5). The azimuth and elevation angles determine the laser orientation while the twist angle determines the camera twist positions. The ratio of baseline distance and standoff distance corresponds to the radius of the circles. The laser vector corresponds to the center of the circle, with the two camera vectors corresponding to two points on the two circles. Note that the two camera positions are off by a fixed angle around the laser source position, depending on the actual position of two cameras. In the situation shown in Fig. 2, they are off by 180 deg. For a given point P on the Gaussian map, there are three distances: distance $d1$ between point P and right camera vector, $d2$ between P and left camera vector, and $d3$ between
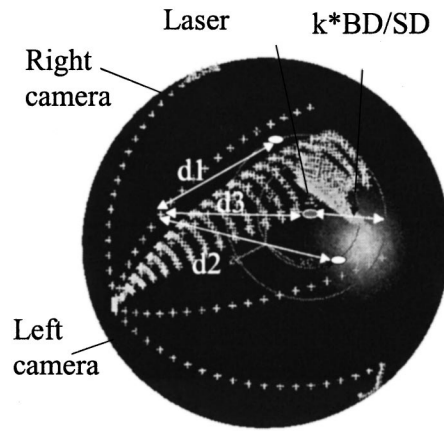

Fig. 5 Setup parameters in a Gaussian map.

P and laser vector. They respectively correspond to the right camera view angle, left camera view angle, and laser incidence angle. The angles can be calculated via

$$\theta = 2 \sin^{-1} \frac{d}{2}.$$

The impact of the standoff distance and baseline distance change over dynamic range variation can be easily deduced. That is, under the constraints of sensor sensitivity and geometric magnification error, the larger the distances are, the smaller the signal dynamic range is. These distances are primarily determined by optical constraints other than dynamic range. So in this paper, we focus on the orientation's impact on signal dynamic range.

Therefore, the best setup issue has been transformed into an issue of finding an optimal configuration on a sphere so that the camera 1 view angle distance $d1$ and camera 2 view angle distance $d2$ are minimized. That is, for a given SD and BD, we need to have the following optimization:

$$\min\{\max[d1(\theta_{\text{twist}}, \theta_{\text{azimuth}}, \nu_{\text{elevation}})_i,$$

$$d2(\theta_{\text{twist}}, \theta_{\text{azimuth}}, \nu_{\text{elevation}})_i]\}.$$

The maximum view angle distance for each camera needs to be minimized. This is a minimal maximum problem. Typical gradient methods only give local optimal solutions. In order to minimize dynamic range, we may naively calculate these angles for all the points on the surfaces for all configurations and then optimize it. This is computationally prohibitive. Therefore, in this paper, we use spherical convex hull (SCH) to find out the points that may lead to maximal signal dynamic range instead of calculating dynamic range for each point on the surface.

Once the spherical convex hull is obtained, a method is needed to find the best (lowest) camera view angles. For multiple cameras, finding the best camera view angles is a complex and nonlinear problem. It is also a minimal maximum problem since we want to ensure the maximum angle distance of all the cameras to be minimized. Even though the variable space is simplified to a spherical convex hull, the objective function is still a minimal maximum problem,
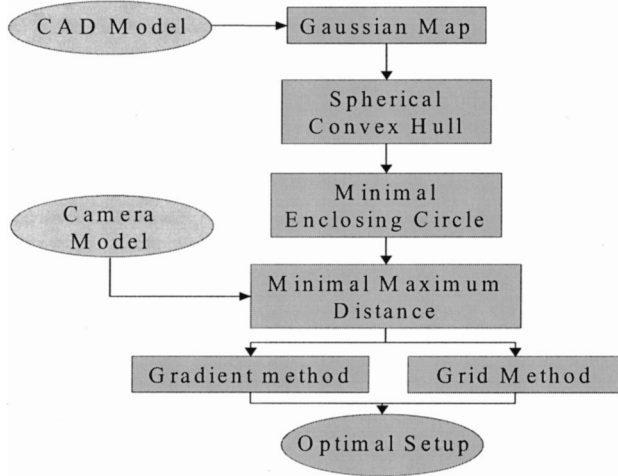
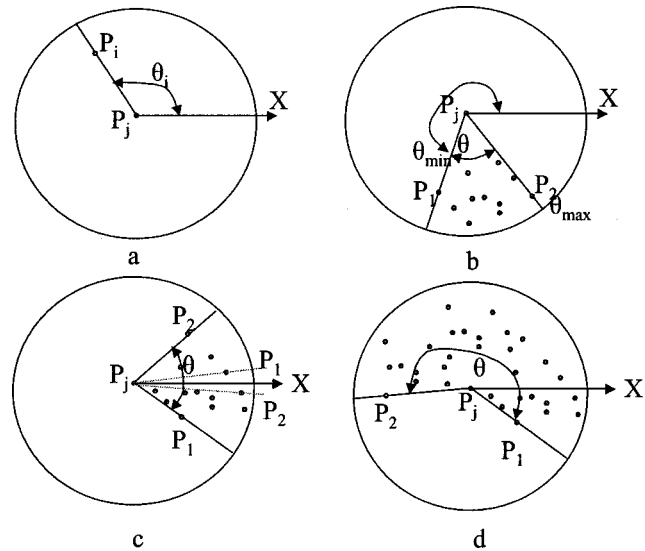**Fig. 6** Procedures for optimal sensor setup.

Fig. 7 Angle span of point set S at point P.

so an efficient optimization method is needed. In order to overcome local optimum, first we use geometric reasoning to obtain a near-optimal solution. We then use a numerical iterative method to obtain the optimal solution.

The overall procedures are shown in Fig. 6. For a given part to be measured, it is first discretized to obtain a point cloud and its Gaussian map. In order to simplify the calculation of maximum angle distance between cameras and points on the surface, we calculate the spherical convex hull. Next, a minimum enclosing circle containing all the surface normals is found. We use the minimal enclosing circle to find the minimal laser incident angle. Under this condition, we use an algorithm for minimal maximum angle distance to analytically find the camera orientations. This gives us the near-optimal orientation. We then use the gradient method with perturbation to find a free-optimal orientation under which there exists the best possible camera view angles. Finally, a grid method is employed to find a constrained optimal solution where the optical constraints are satisfied.

In this paper, we make distinctions of four orientations: near-optimal, free-optimal, constrained-optimal, and existing orientations.

Near-optimal orientation refers to an orientation that has the minimal camera view angle under the condition of minimal laser incident angle. The center of the minimal enclosing circle determines the azimuth and elevation angles of the laser. When the laser is fixed at the center of the minimal enclosing circle, the camera twist obtained by the angle distance optimization is the best camera angle possible for minimal signal dynamic range under the optimal laser angle. In this orientation, the laser incident angle is minimal.

Free-optimal orientation refers to the best orientation for the minimal camera view angles. This orientation corresponds to the best orientation for minimizing the signal dynamic range. In this orientation, the laser angle may not be minimal.

Constrained-optimal orientation refers to the best orientation for low dynamic range and low camera view angle while satisfying the field of view, resolution, and magnification constraints.

Existing orientation refers to the existing orientation used before optimization.

4 Computational Approach for Optimal Sensor Setup

4.1 *Hemispherical Test and Spherical Convex Hull*

To simplify the calculation of maximum camera view angles and maximum laser incident angles for all the points on the part surfaces, we use the spherical convex hull of surface normals. The first step of finding a spherical convex hull is to determine whether the point set of surface normals lies on a hemisphere. We propose the use of the angle span of a point set to decide whether the point set on a sphere is hemispherical. Further, if it is hemispherical, we use a rotating "cutting plane" method to form the spherical convex hull.

4.1.1 *Hemispherical test*

By definition, if a point set is not hemispherical, its spherical convex hull is the whole sphere.[8] In practice, since all the visible points have view angles smaller than 90 deg, they all lie on a hemisphere. Therefore a general hemispherical test is needed to obtain the spherical convex hull for the situations where the SCH is not the whole sphere surface.

For a given point p_j, $(x_{p_j}, y_{p_j}, Z_{p_j})$, in the point set S of surface normals, there is a principal plane P_p going through $(0,0,0)$ and with normal $(x_{p_j}, y_{p_j}, z_{p_j})$. If we project all the points in the set S onto the plane along the direction $\overrightarrow{op_j}$, we get the projected point set S'. For any point q in S', $\overrightarrow{p_jq}$ forms a vector. The point set $S's$ angle span at point p_j is defined as the minimal angle of two vectors starting from point p_j and bounding all the vectors $\overrightarrow{p_jp_i}$, $i=1, n$, and $p_j \neq p_i$. The angle between $\overrightarrow{p_jp_i}$ and the x axis is $\theta = a\cos(\overrightarrow{p_jp_i}\cdot\vec{x})$. For any point $p_i \in S$, $i \neq j$, there is such an angle θ_i as shown in Fig. 7(a). Clearly, angle span is independent of the choice of x axis.

The procedures for obtaining the angle span of a point set S of surface normals at point p can be divided into three steps:

1. Project all the points on the p_j's principal plane P_{p_j}.

2. Calculate the angle difference $\Delta\theta$. Let θ_{max} and θ_{min} be the low and high bound angles, $\Delta\theta = \theta_{max} - \theta_{min}$.

3. Calculate the amended angle difference $\Delta\theta'$ if the angle difference $\Delta\theta$ obtained in step 2 is larger than 180 deg. For any angle $\theta < 180$ deg, it is amended by the addition of 360 deg, i.e., $\theta' = \theta + 360$. If we denote the maximum and minimal amended angles as θ'_{max} and θ'_{min}, we have $\Delta\theta' = \theta'_{max} - \theta'_{min}$. Angle span is $AS = \min(\Delta\theta, \Delta\theta')$.

In Fig. 7(a) point p and set S are on a unit sphere. In Fig. 7(b) points are projected to principal plane P_{pj}. In Fig. 7(b), $\overrightarrow{p_jp_1}$ and $\overrightarrow{p_jp_2}$ are two bounding vectors. In Fig. 7(c), the angle span is the angle between $\overrightarrow{p_jp_1}$ and $\overrightarrow{p_jp_2}$, not the angle between $\overrightarrow{p_jp_1'}$ and $\overrightarrow{p_jp_2'}$, since the angle between $\overrightarrow{p_jp_1'}$ and $\overrightarrow{p_jp_2'}$ is larger than 180 deg.

With the above definition of angle span, we have the following lemma for the hemispherical test.

Lemma 1: If one point in a point set has an angle span less than 180 deg, the point set is hemispherical. If none of the points has an angle span less than 180 deg, the point set is nonhemispherical (hemispherical test).

The pseudocode algorithm for the hemispherical test can be described as follows:

Algorithm 1: An angle span based hemispherical test

Input: surface normal point set S
Output: whether S is hemispherical
For each point p_i in S
  Calculate its principal plane P_{p_i}
  For all the points p_j in S, j=1…n, j≠i
    Project p_j onto plane P_{p_i}
    Calculate angle θ_j with respect to an X-axis
  Endfor
  Find the angle difference $\Delta\theta = \theta_{max} - \theta_{min}$. If $\Delta\theta$ <180, return true.
  For all the points p_j in S, j=1…n, j≠i
    Amend the angle $\theta_j = \theta_j + 360$ if $\theta_j < 180$
  Endfor
  Find the amended angle difference $\Delta\theta' = \theta'_{max} - \theta'_{min}$
  If $\Delta\theta'_i < 180$, return true.
ENDFor
Return False

The hemispherical test has the worst case complexity of $O(n^2)$ when the point set S is not hemispherical, but is far easier to implement. If the spherical polygon is hemispherical, its computational complexity is expected to be $O(n^2/F)$ where n is the size of point set S and F is the number of convex points of S.
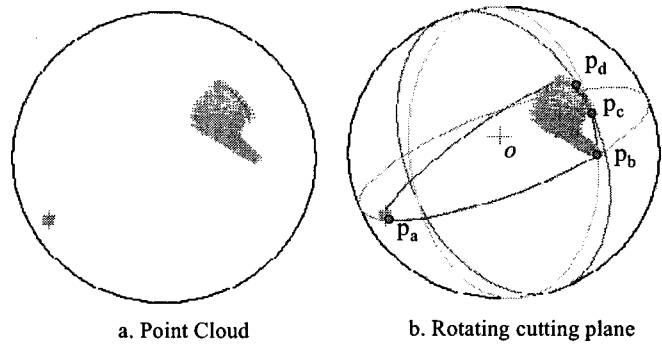

a. Point Cloud   b. Rotating cutting plane

Fig. 8 Rotating cutting plane for spherical convex hull.

4.1.2 Rolling cutting plane method for spherical convex hull

Based on the angle span concept, we have the following lemma to obtain convex points on the spherical convex hull.

Lemma 2: For a hemispherical point set S, a point $p \in S$ is a convex point on the spherical convex hull if and only if the angle span of the point set S at point P is less than 180 deg (spherical convex hull).

From the hemispherical test, we can have one point p_j, upon its principal plane P_{p_j}; the rest of the points have an angle span smaller than 180 deg. Let us denote a cutting plane going through three points: point p_j, point p_i, which has the minimal bounding angle, and the origin point o. This cutting plane cuts the sphere into two parts. If we let the normal of the plane point to $\overrightarrow{op_j} \times \overrightarrow{op_i}$, the point set S lies on the left side of plane. If we obtain the principal plane of point p_i and project all the points on the principal plane of p_i, then the point that has minimal angle is the next convex point. We can repeat this process until all the convex points are found.

Figure 8 shows how the spherical convex hull of a set of point cloud can be obtained by this method. Figure 8(a) shows the Gaussian map of the airfoil and platform surfaces of a turbine blade. On the principal plane of point p_a, $\overrightarrow{p_ap_b}$ forms the low bound of the point set. So p_b becomes the convex point. On the principal plane of p_b, p_c has the minimal angle, so p_c becomes the next convex point. This process repeats until the first point p_a is hit. Every time a new minimal angle point is found, a cutting plane is formed. For example, corresponding to the points p_b, p_c, and p_d are planes op_ap_b, op_bp_c, and op_cp_d. We refer to this method of rotating the principal plane to obtain SCH as a rotating cutting plane method.

So we have the following algorithm for obtaining the spherical convex hull.

Algorithm 2 for Spherical Convex Hull

Input: a point set S of surface normals
Output: spherical convex hull (SCH) of the set S
  1. for each point in the point set of the surface normals
    a. calculate its angle span.
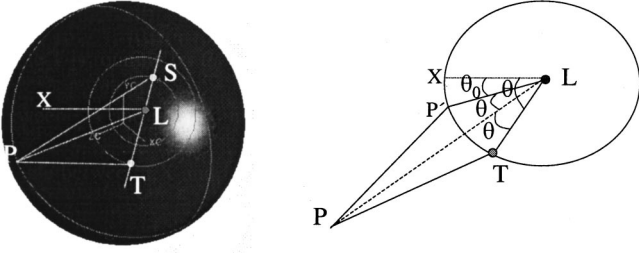   *b. If angle span is less than 180, record the convex point as p, break;*

Fig. 9 Angle distance calculation.

> c. Else, continue.
>   endfor
> 2. if no convex point p is found, it is not hemi-spherical, return the whole spherical surface
> 3. record point p as first convex point and add it to SCH
> 4. find the low bound point q from the convex point p's principal plane
> 5. if q is the same point as first convex point, the complete convex hull is found and return SCH;
> 6. otherwise, add q into SCH and record q as p and goto step 4

The complexity of the algorithm is $O(n^2)$ and n is the number of points in S. This spherical convex hull algorithm has the worst complexity $O(nF)$ if an initial convex point p is given.

4.2 Minimal Enclosing Circle

Once we find SCH, we need to get an orientation that gives minimal camera view angles for all the cameras. In order to overcome the local optimum, we use a near-optimal orientation as the initial position for iteration. This near-optimal orientation corresponding to minimal laser incident angle can be obtained analytically using a geometric reasoning method. This minimal laser incident angle corresponds to a laser vector L, which has the minimal distance d to reach all the surface points on the Gaussian map. This laser vector L corresponds to the center of the minimal enclosing circle. We use an algorithm[10] to obtain minimal enclosing circle, which has a complexity of $O(n \log n)$.

4.3 Minimal Maximum Angle Distance Algorithm

In this section, we present an algorithm for analytically obtaining the minimal camera view angles for all the cameras under the fixed laser orientation. The algorithm is applicable to a larger number of cameras.

In Fig. 9, point L represents the laser vector, and points S and T represent two camera vectors. As shown in Fig. 2, the laser source lies in the plane formed by the two principal axes of the two cameras. Therefore, OS and OT are off by 180 deg in Fig. 9. For a point P that lies on the spherical convex hull, the arc distance such as PS and PT represents the angle between the surface point normal and camera principal axes. These camera view angles can be calculated from the Eucludian distance $\|PS\|$ and $\|PT\|$. That is,

$$\theta_s = 2 * \sin^{-1}\left(\frac{\|PS\|}{2}\right) \quad \text{and} \quad \theta_T = 2 * \sin^{-1}\left(\frac{\|PT\|}{2}\right).$$

To minimize the signal dynamic range, we assume point L is fixed in this step, which corresponds to the SCH's minimal enclosing circle center. At this point, the laser angle is minimal and the cameras S and T can rotate around point L on their respective circles. We need to find an optimal camera twist so that the larger one of $\|PS\|$ and $\|PT\|$ is minimal. We draw an arbitrary axis LX so that $LX \perp OX$ and O is the origin point of the unit sphere. The angle distance between a point P on the spherical polygon and the camera T while T is rotating on the circle can be described by a function of θ, where θ is the angle between LX and LT. Point P is projected to point P' on the plane of points (L, X, T). The angle between LX and LP' is denoted as θ_0, the angle between LP and LP' as β. For a given point P and the camera center T and the chosen point X, θ_0 and β are known by the following equations:

$$\theta_0 = \cos^{-1}\left(\frac{\overrightarrow{LX}}{\|LX\|} \cdot \frac{\overrightarrow{LP'}}{\|LP'\|}\right),$$

$$\beta = \cos^{-1}\left(\frac{\overrightarrow{LP}}{\|LP\|} \cdot \frac{\overrightarrow{LP'}}{\|LP'\|}\right).$$

The angle between LP and LT can be obtained from the following equation:

$$\cos \alpha = \cos(\theta - \theta_0) \cdot \cos \beta. \tag{3}$$

So the camera T's angle distance to point p is

$$\|PT\|^2 = \|PL\|^2 + \|LT\|^2 - 2 \cdot \|PL\| \cdot \|LT\| \cdot \cos \alpha_T. \tag{4}$$

A similar equation can be derived for camera S:

$$\|PS\|^2 = \|PL\|^2 + \|LS\|^2 - 2 \cdot \|PL\| \cdot \|LS\| \cdot \cos \alpha_s.$$

If we substitute Eq. (3) into Eq. (4), we have camera view angles as a function of θ:

$$\|PT\|^2 = \|PL\|^2 + \|LT\|^2$$
$$- 2 \cdot \|PL\| \cdot \|LT\| \cdot \cos(\theta - \theta_0) \cdot \cos \beta. \tag{5}$$

So the angle distance can be abbreviated as $d = a \cos(\theta_{\text{Twist}} - \theta_0) + b$ for a given point P, in which

$$a = -2\|PL\| \cdot \|LT\| \cdot \cos \beta, \tag{6}$$

$$b = \|PL\|^2 + \|LT\|^2. \tag{7}$$

Thus, each convex point in SCH has a distance function similar to Eq. (5). When the camera twist angle changes from 0 to 360 deg, i.e., camera T and S can rotate around L for the whole circle, each function describes the angle distance of camera T and S to the point. If we intersect all the functions and find the maximum angle distance function for each intersection interval, we can obtain the maximum angle distance from T and S to all the convex points when T and S rotate from 0 to 360 deg.
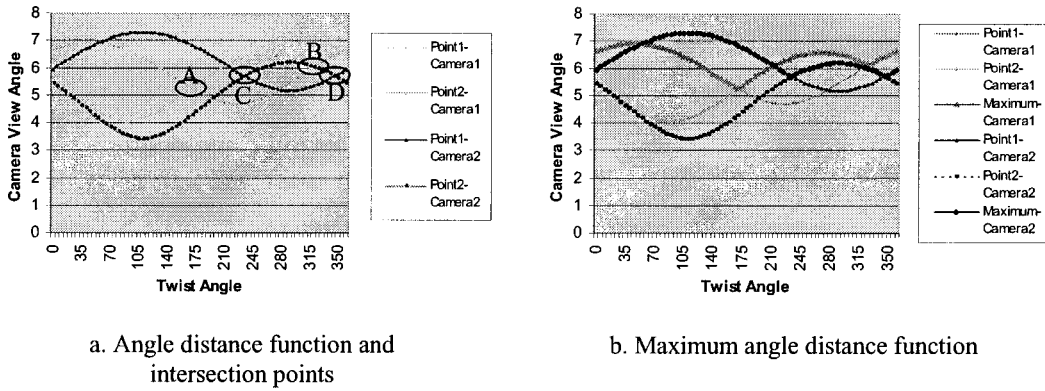
a. Angle distance function and
intersection points

b. Maximum angle distance function

Fig. 10 Angle distance function and intersection.

The detailed procedures for obtaining minimal maximum camera view angle distance are described in the following. We use two cameras S and T to illustrate each step.

Step 1: Obtain camera angle distance functions. For given points P and Q on the spherical polygon and two cameras S and T, we can have the angle distance functions represented as $d = a \cos(\theta_{\text{Twist}} - \theta_0) + b$. The exact values of a, b, and θ_0 are functions of the point P and laser vector L and camera circle S or camera circle T, as described in Eq. (6) and Eq. (7). For n number of points in the spherical polygon and m cameras, we will have nm angle distances. Figure 10(a) illustrates such functions when $n=2$, $m=2$.

Step 2: Intersect angle distance function and obtain maximum angle distance. In this step, there are two subtasks. Subtask 1 is to intersect all the angle distance functions and to obtain the intersection points. Subtask 2 is to obtain the maximum camera view angle distance functions among all cameras when the twist angle changes from 0 to 360 deg.

For a camera and any point on the spherical polygon, there is a distance function $d = a \cos(\theta_{\text{Twist}} - \theta_0) + b$. For any two points, p and q, on the polygon, we have two distance functions, noted as $d_p = a_p \cos(\theta_{\text{Twist}} - \theta_{0_p}) + b_p$ and $d_q = a_q \cos(\theta_{\text{Twist}} - \theta_{0_q}) + b_q$. To intersect d_p and d_q, we have

$$a_p \cos(\theta_{\text{Twist}} - \theta_{0_p}) + b_p = a_q \cos(\theta_{\text{Twist}} - \theta_{0_q}) + b_q.$$

If we expand it, we have

$$(a_p \cos \theta_{0_p} - a_q \cos \theta_{0_q}) \cdot \cos \theta_{\text{Twist}} - (a_p \sin \theta_{0_p}$$
$$- a_q \sin \theta_{0_q}) \cdot \sin \theta_{\text{Twist}} = b_q - b_p.$$

Denote $A = a_p \cos \theta_{0_p} - a_q \cos \theta_{0_q}$, $B = a_p \sin \theta_{0_p} - a_q \sin_{0_q}$, and $C = (b_q - b_p)/(A^2 + B^2)^{1/2}$. So two intersection points would be at

$$\theta_{\text{Twist}} = \pm a \cos(C) + a \tan(B/A).$$

The intersection points of two distance functions are also shown in Fig. 10(a) for two cameras. Points A and B are the

intersection points for two distance functions of points 1 and 2 with camera 1, and points C and D are intersection points for camera 2. The complexity of subtask 1 is $O(n^2)$ where n is the number of points in SCH.

The second subtask is to find a maximum angle distance for each camera when the camera twist changes from 0 to 360 deg. For each pair of distance functions, there are two possible intersection points. If a spherical polygon has n vertex, so there are possibly $2 \cdot {}_nC_2$ intersection points and $2 \cdot {}_nC_2 + 1$ intervals between intersection points. For each interval, we need to find the maximum distance function during the interval. For n curves, it will take $n \cdot (2{}_nC_r + 1) \cdot \log(2{}_nC_r + 1) = O(n^3 \log n)$ comparisons to sort the intervals and find the maximum distance function for each interval. To avoid the complexity $O(n^3 \log n)$ of the sorting process, we use the intersection adjacency relationship to speed up the sorting process. That is, during the distance function intersection process, we record the intersection attending functions. If we know function d_p and d_q intersect at point A, let us suppose for $\theta < A$, $d_p(\theta) < d_q(\theta)$; then we know for $\theta > A$, we have $d_p(\theta) > d_q(\theta)$. Therefore, we can use this intersection adjacency relation at point A to speed up the distance function comparison without the need to calculate the function value for each interval.

Subtask 2 involves these three steps: getting the first interval with complexity $O(n^2)$, finding the curve of highest value for the first interval with complexity $O(n)$, and finding this curve's conjugate curve through intersection adjacency relationship $O(n)$. The expected time of finding the conjugate curve is $O(n)$. So the algorithm for subtask 2 has complexity $O(n^2)$ and n is the number of points in the spherical polygon.

The algorithm for the maximum angle distance sorting (subtask 2) is described in Algorithm 3.

Algorithm 3 Maximum Angle Distance Function Sorting
Input: n angle distance curves and the intersection points' adjacency
Output: maximum distance function list for all intervals
1) Find the first smallest intersection point θ_{min}
2) Find the curve C_i that has the highest value during the first interval $(0, \theta_{min})$
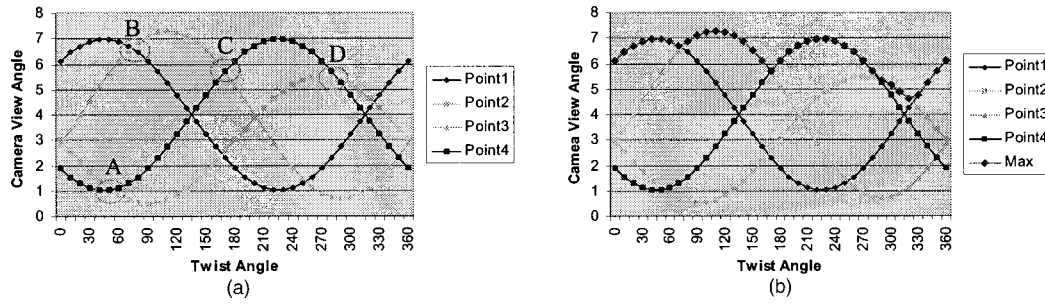
Fig. 11 Intersection adjacency used to speed up the sorting process.

3) *Find curve C_i's smallest intersection θ_i so that $\theta_i \geq \theta_{min}$. Let $\theta_{min} = \theta_i$.*
4) *Add C_i at interval $(0, \theta_{min})$ to the list*
5) *Find curve C_i's next smallest intersection point θ_i so that $\theta_i \geq \theta_{min}$*
6) *Find the conjugate curve C_j of curve C_i, which intersects with C_i at point θ_i*
7) *Add C_j at internal (θ_{min}, θ_i) to the list*
8) *$\theta_{min} = \theta_i$, $C_i = C_j$*
9) *Repeat step 5, step 6, step 7 and step 8 until θ_{min} is 360.*

As shown in Fig. 11(a), the distance function for point 1 has the highest value at first interval. The closest intersection point to the first interval of curve 1 is *B*. Because of the recorded intersection relationship, we know the conjugate intersection curve of curve 1 at point *B* is curve 3. Therefore curve 3 has the highest angle distance during the interval right after point *B*. Likewise, we can infer that curve 4 has the highest value for the intervals between point *C* and point *D*. We can repeat the process until all the intervals' maximum distance functions are found.

Step 3: Offset camera twist. In accordance with our previous description, camera twists for camera *S* and *T* are off by 180 deg. We offset the maximal distance function for camera 1 and camera 2 and obtain the results. Figure 12(a) shows the maximum angle distance function for two cameras. After the function for camera 2 is shifted by 180 deg, the two functions are shown in Fig. 12(b).

Step 4: Obtain minimal maximum camera angles. In this step, we intersect the two maximum angle distance functions for two cameras and obtain the maximum camera

angle distance for two cameras when the camera twist angle changes from 0 to 360 deg. The complexity of this step is $O(n)$ where n is the number of points on the SCH. A point on the maximum distance curve that has the lowest value corresponds to the optimal twist angle, as shown in point *A* in Fig. 12.

So the algorithm for analytically obtaining the minimal camera view angles can be summarized using the following pseudocode:

Algorithm 4 Minimal Maximum angle distance
Input: n convex points in the SCH, m cameras and the relative $\Delta\theta_i$ among the cameras
Output: twist angle for the maximal camera view angles to be minimal for m cameras
Algorithm:
For each camera C_i, $i = 1...m$
  For each convex point p_j, $j = 1...n$
    Calculate camera C_i's view angle distance function d_{ij}
  Endfor
  Intersect all the distance functions d_{ij}, $j = 1..n$ and obtain the maximum distance function D_{ci} for camera C_i (See Algorithm 3).
  Shift maximum distance function M_{ci} by $\Delta\theta_i$
Endfor
Intersect all the maximum distance functions M_{ci}, $i = 1...m$ and obtain the maximum angle distance function M_C for all the cameras (See Algorithm 3)
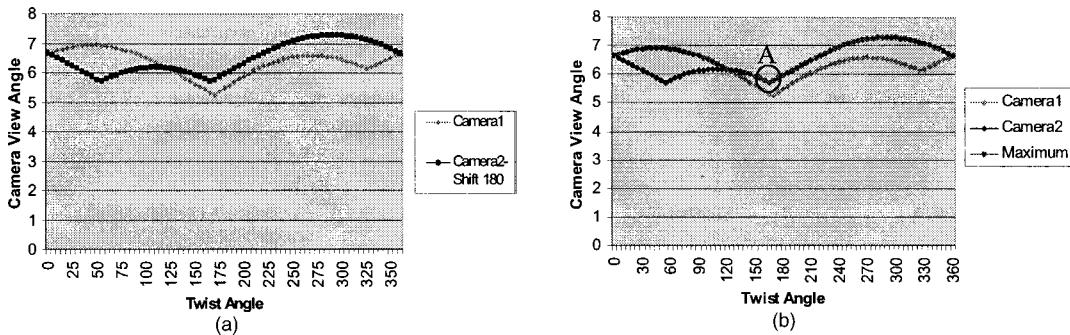

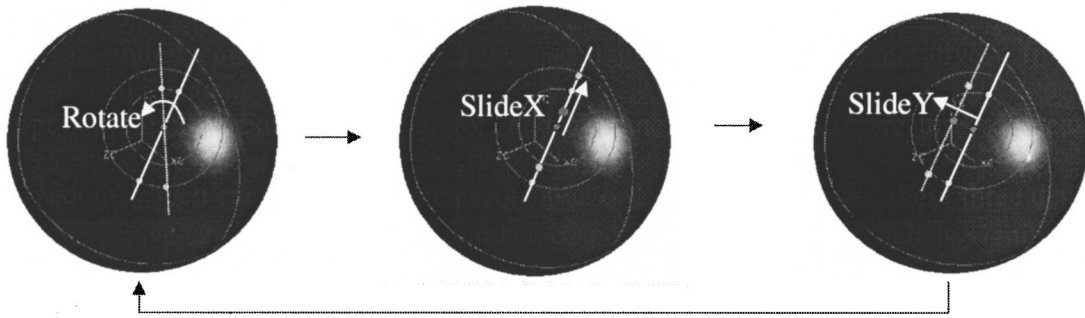**Fig. 12** Offset camera twist and obtain minimal maximum angle distance.

Fig. 13 Gradient method for minimal camera view angles.

Return the angle θ that has the minimal angle distance.

In the above algorithm, n is the number of points in the SCH, which is significantly smaller than the number of points on the surface. The complexity is $O(n^2m)$ and m is the number of cameras.

4.4 Gradient and Grid Methods for Optimal Setups

The sections above describe a method to find a near-optimal solution, which has the lowest camera view angle under the condition of minimal laser incident angle. The optimal orientation where the maximum camera view angles are minimal may not happen at this initial condition. Therefore, we use a gradient method to iteratively find the optimal solution. For a given standoff and baseline distance, there are three degrees of freedom, which can be changed in a sequential order. We decompose these three degrees of freedom into the following three movements: slide X, slide Y, and rotation as described in Fig. 13. For given orientations of camera S and T, there exists a plane that passes through three points O, S, and T; X is defined to be on this plane and perpendicular to OL, while Y is defined to be perpendicular to this plane and is going through to OL. Rotation is to change the twist angle around L as described in Sec. 4.3.

The advantage of this decomposition is that for each degree of freedom, we can obtain an analytical solution to minimize the cameras' view angle. The detailed iteration is described as follows. From the near-optimal solution we obtained the following solution:

- Find an optimal angle delta $\Delta\theta_x$ along the slide X direction so that the camera view angle for all the cameras is minimal.
- Find an optimal angle delta $\Delta\theta_y$ along slide Y, so that the camera view angle is minimal.
- Find the optimal rotation angle. This can be obtained using Algorithm 4.
- If a local optimal solution is reached, a perturbation is added to slide X, slide Y, or rotation. Repeat the above process until it converges.

After we obtain the optimal setups for the minimal camera view angle and minimal laser incident angles, we use a grid method to obtain the constrained optimal. The configuration space of five degrees of freedom is gridded near the optimal orientation, and an orientation is found that has the minimal camera view angle while satisfying all the optical constraints.

5 Implementation and Experimental Result

An optimal sensor setup system based on the above methodology has been implemented. Given a part model to be inspected and the basic optical characteristics of the measurement system, the system can automatically calculate the optimal sensor setup for minimizing signal dynamic range. For example, for the blade shown in Fig. 2, four orientations and the respective optical characteristics calcu-
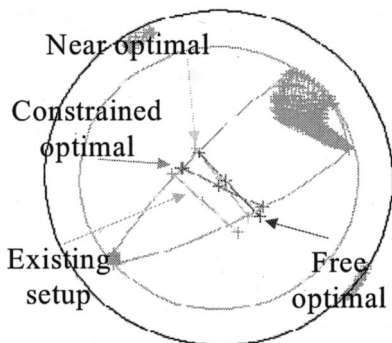

Fig. 14 Four orientations in a spherical map.

Table 1 Comparison of optical characteristics under different orientations.

|	Existing	Near optimal	Free optimal	Constrained optimal
Elevation,	37	45.8427	45.8427	45.8427
Azimuth,	55	45.9761	35.9761	37.9761
Twist	0	−4.0881	1.91182	7.91182
Dynamic Range	93.257	50.8218	43.3905	46.9631
Sensitivity	0.000569	0.00039	0.00034	0.001217
Camera 1 Angle	68.175	55.3258	51.5178	53.9075
Camera 2 Angle	57.932	51.9584	53.9564	54.696
Laser angle	60.3499	50.5844	51.0399	50.9602
Delta DOF	0.404982	0.37395	0.48252	0.387748
% Magnification	7.50915	6.92779	8.96652	7.1861
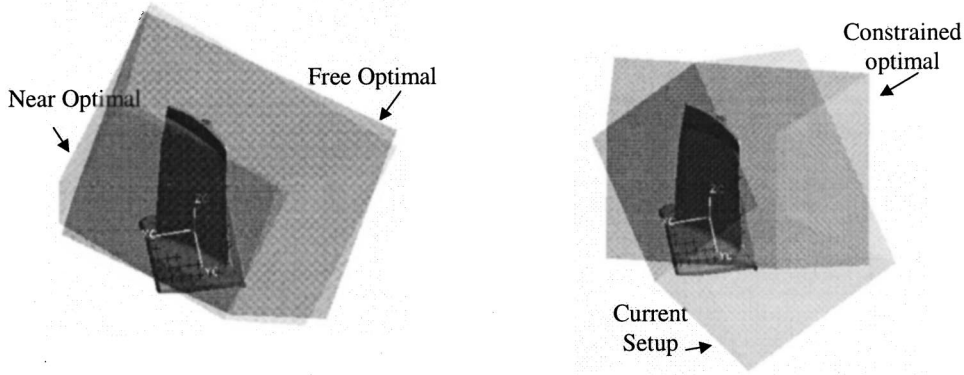
Fig. 15 Measurement volume comparison.

lated by the system are shown in Fig. 14 and Table 1. These four orientations are the existing setup, the near-optimal setup obtained by solely geometric reasoning, i.e., minimal enclosing circle and minimal maximum angle distance calculation, the free-optimal setup with no optical constraints, and the constrained-optimal setup. The four orientations' relative positions in the Gaussian map of the blade are shown in the Gaussian map (Fig. 14). As revealed in the figure, the angle distance between the cameras and platform surface in the existing setup is smaller than the angle distance between the camera and airfoil. That is to say, the current setup before optimization is biased against the platform surface.

Table 1 lists different optical characteristics under four orientations. The items in the table include setup orientations, dynamic range, sensitivity, maximum right camera view angle, maximum left camera view angle, maximum laser incident angle, depth-of-field difference, and percentage of geometric magnification error. As shown in Table 1, all three optimal orientations give lower signal dynamic range than before optimization. The near-optimal orientation gives the lowest laser incident angle (53.38), while free-optimal orientation gives the lowest camera view angle (53.03), which results in the lowest signal dynamic range (42.06). Constrained-optimal orientation gives good signal dynamic range while satisfying optical constraints such as sensitivity and depth-of-field difference.

Figure 15 shows the part's position relative to the measurement volumes under four orientations. This is used to check whether a part is out of the measurement volume under a particular orientation.
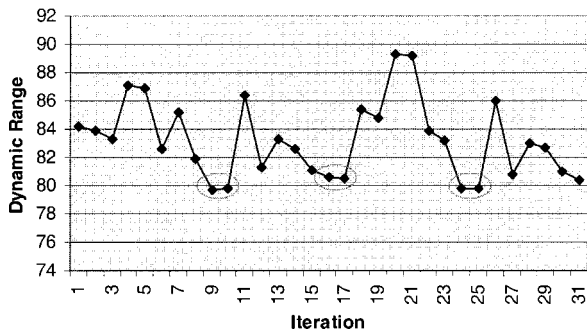
Figure 16 shows that the gradient method with perturbation along three directions gives the optimal solution for a different blade part. The optimal dynamic range obtained by the grid method is 80.87. With two or three iterations, this gradient method gives a solution very close to the optimal solution.

The dynamic range variation with the three orientation angles is shown in Fig. 17. As the figure shows, any deviation from the optimal orientation leads to higher signal dynamic range.

In order to validate the overall methodology presented in this paper, we conducted an experiment on parts with shiny spots. Figure 18 illustrates how the model coverage changes over different orientations. The spots circled in the figures are shiny. The top row is measurement at the elevation angle of 30 deg and the bottom row at the elevation angle of 42 deg. Across each row is the measurement at different azimuth angles from 45 to 70 deg. By the optimization of the sensor setup, the model coverage has been improved as predicted.

6 Conclusion

In this paper, we presented a methodology for the optimal sensor setup for an optical metrology system. In particular, the signal dynamic range received by the cameras is minimized by the optimization of the sensor/part relative position. On the computation side, we developed novel algorithms on a spherical map for obtaining the spherical convex hull using the angle span and the rotating cutting
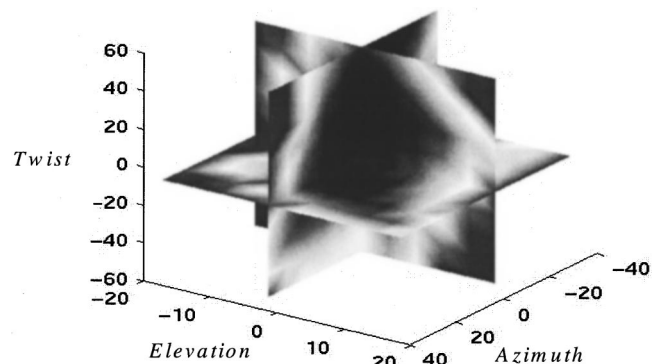

Fig. 16 Gradient method with perturbation.

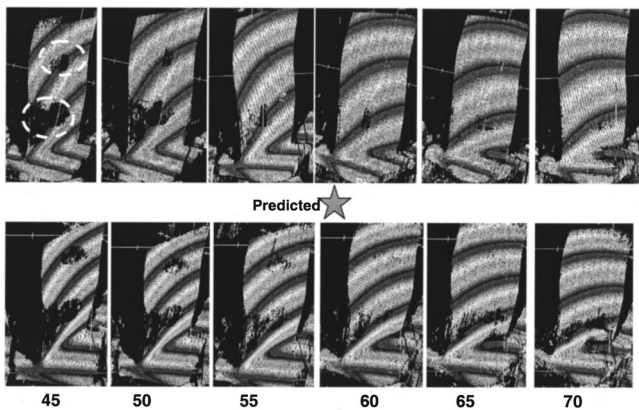**Fig. 17** Dynamic range vs sensor orientation.

Fig. 18 Model coverage vs orientation.

plane method. We also developed an effective method for calculating minimal maximum camera view angles on a unit sphere. The near-optimal analytical solution is obtained via geometric reasoning, then the constrained optimal solution is obtained by numerical iteration. On the optical side, we developed a methodology for minimizing signal dynamic range by optimizing the sensor setup. This is especially useful for the measurement of shiny surfaces. Experimental results were presented that validated the prediction from the model.

This methodology is directly applicable to multiple sensor systems, in which multiple cameras need to be simultaneously optimized to receive minimal signal dynamic range. This methodology can be further extended for sensor design, where different performance measures such as depth of field, magnification error, and resolution need to be verified for a particular part inspection. This method can also be used for stage design for large part measurement where the motion envelope of the sensor/part can be derived based on the optimal setup.

Acknowledgments

References

1. K. G. Harding, "Current state-of-the-art of contouring techniques in manufacturing," *J. Laser Appl.* **2**(2&3), 41–48 (1990).
2. R. F. Rauchmiller, K. G. Harding, M. A. Michniewicz, and E. A. Kaltenbacher, "Design and application of a lighting test bed," *SME Vision '90*, MI, pp. 1–14, Detroit, MI (1990).
3. K. G. Harding, "Future trends in laser gaging," *Proc. SME Laser Gaging Methods and Technologies*, Detroit, MI (1995).
4. K. G. Harding, "Speckle reduction methods for laser line gages," in *Three-Dimensional Imaging and Laser Based Systems for Metrology and Inspection III*, K. Harding, Ed., *Proc. SPIE* **3204**, 137–144 (1997).
5. K. A. Tarabanis, R. Y. Tsai, and P. K. Allen, "The MVP sensor planning system for robotic vision tasks," *IEEE Trans. Rob. Autom.* **11**(1), 72–85 (1995).
6. S. Yi, R. M. Haralick, and L. G. Shapiro, "Optimal sensor and light source positioning for machine vision," *Comput. Vis. Image Underst.* **61**(1), 122–137 (1995).
7. Y. P. Orly, "Wide-dynamic-range sensors," *Opt. Eng.* **38**(10), 1650–1660 (1999).
8. L. L. Chen and T. C. Woo, "Computational geometry on the sphere with application to automated machining," *ASME J. Mech. Des.* **114**, 288–295 (1992).
9. C. Y. Chou, L. L. Chen, and T. C. Woo, "Separating and intersecting spherical polygons: computing machinability on three, four and five-axis numerically controlled machines," *ACM Trans. Graphics* **12**(4), 305–326 (1993).
10. J. G. Gan, T. C. Woo, and K. Tang, "Spherical maps: construction, properties, and approximation," *ASME J. Mech. Des.* **116**, 357–363 (1994).
11. R. K. Arni and S. K. Gupta, "Manufacturability analysis of flatness tolerances," *ASME J. Mech. Des.* **123**(1), 148–156 (2001).
12. G. Elber and E. Zussman, "Cone visibility decomposition of freeform surfaces," *Comput.-Aided Des.* **30**(4), 315–320 (1998).
13. T. S. Smith and R. T. Farouki, "Gauss map computation for free-form surfaces," *Computer Aided Geometric Design* **18**, 831–850 (2001).
14. R. Kinsely, *Optical System Design*, p. 121, Academic Press, New York (1983).

Xiaoping Qian received his BS and MS degrees in mechanical engineering in 1992 and 1995 from Huazhong University of Science and Technology, China. He received his PhD degree in mechanical engineering in 2001 from the University of Michigan, Ann Arbor. Since July 2001, he has been with GE Global Research Center, Niskayuna, New York. His research interests include solid modeling, computer-aided design, computer-aided manufacturing, and computer vision.

Kevin G. Harding has published over 100 technical papers, taught over 50 short courses and tutorials to industrial and academic audiences, as well as an NTU video course on optical metrology, contributed sections to 6 books, and received 16 patents. He has served as conference chairman for over 15 years working with the SPIE, LIA, ESD, SME, and OSA, as well as served as a frequent topical reviewer in interferometry for *Applied Optics*. He was one of the directing principal investigators on the National Science Foundation's National Alliance for Photonics Education in Manufacturing (NAPEM) for 5 years, as well as serving as an industry advisor to Ketting University, University of Michigan Sam Wu Technology Center, and the Ann Arbor, MI Schools industry liaison program. He is currently working at GE Global Research Center.